Validation of Integrated EV Chassis Controller Using a Geographically Distributed X-in-the-loop Network

Beliautsou, Viktar ; Alfonso, Jesus ; Giltay, J.N.P.; Büchner, Florian ; Shyrokau, B.; Castellanos, Jose A. ; Ivanov, Valentin

DOI
10.1109/VPPC55846.2022.10003267

Publication date
2022

Document Version
Final published version

Published in
Proceedings of the 2022 IEEE Vehicle Power and Propulsion Conference (VPPC)

Validation of Integrated EV Chassis Controller Using a Geographically Distributed X-in-the-loop Network

Viktar Beliautsou
Automotive Engineering Group
TU Ilmenau
Ilmenau, Germany
ORCID 0000-0002-2071-1198

Jesus Alfonso
Mechatronics Dept.
Instituto Tecnologico de Aragon
Zaragoza, Spain
ORCID 0000-0001-8080-7696

Joris Giltay
Dept. of Cognitive Robotics
Delft University of Technology
Delft, Netherlands

Florian Büchner
Automotive Engineering Group
TU Ilmenau
Ilmenau, Germany
ORCID 0000-0002-5839-1193

Barys Shyrokau
Dept. of Cognitive Robotics
Delft University of Technology
Delft, Netherlands
ORCID 0000-0003-4530-8853

Jose A. Castellanos
Instituto de Investigación en Ingeniería de Aragón
Universidad de Zaragoza
Zaragoza, Spain
ORCID 0000-0001-5977-8720

Valentin Ivanov
Automotive Engineering Group
TU Ilmenau
Ilmenau, Germany
ORCID 0000-0001-7252-7184

2022 IEEE Vehicle Power and Propulsion Conference (VPPC) | 978-1-6654-7587-7/22/$31.00 ©2022 IEEE | DOI: 10.1109/VPPC55846.2022.10003267

***Abstract*—This paper presents the validation of an integrated chassis controller that unites three groups of actuators for the electric vehicle (EV) with independent in-wheel electric motors (IWMs) for each wheel. Controlled actuators are the IWMs, the active suspension, and the braking system. The models of test benches and the designed architecture of the X-in-the-loop network are presented. The proposed design approach allows testing the developed controller on a vehicle model in real-time and on hardware components.**

***Index Terms*—Control System, Testing processes, X-in-the-Loop (XIL), Hardware-in-the-loop (HIL), Electric vehicle, In-wheel motor**

I. Introduction

Various motion control systems can essentially enhance safety, energy efficiency, and handling of electric vehicles. In the case of EV with individual on-board or in-wheel motors, a key element of such systems is the targeted power distribution between driving or braking wheels to achieve better energy efficiency and safety [1], [2], [3]. In addition, the EV motion control systems can also improve driving comfort, especially through the combination of the active suspension and the powertrain control [4]. Precise torque control of electric motors is also beneficial for the performance of the wheel slip control and the anti-lock braking system [5], [6]. The further improvements in this area can be related to the integrated and coordinated vehicle motion control with several vehicle systems as actuators [7], [8], [9]. This allows for achieving a simultaneous effect in safety and comfort however the control strategy becomes more complicated. Therefore, the integrated control has stronger requirements for such aspects as redundancy and fail-safety [10].

The integrated EV motion control has a demand for new design and testing procedures. Methodologies like hardware-in-the-loop [11], [12] make the design process easier but cannot solve all the challenges of comprehensive vehicle development and validation. The potential solution can be in the organisation of collaborative design through groups of developers from different locations, with the possibility of real-time simultaneous experimental procedures accompanied by data exchange between the groups. Such an approach calls for the implementation of more complex techniques such as network-based X-in-the-loop (XIL) [13], [14].

Another challenge is to reach the full potential offered by highly dynamic powertrain and chassis actuators. This can be beneficial for extended functionality and redundancy of motion control [10], [15].

To investigate a complex system such as an integrated chassis controller (ICC) characterized by a large number of settings and parameters, it is essential to have high-fidelity component models in order to ensure the best possible control performance [14]. In this case, the strategy has the targets not only to control the actuators but also to select their range for optimal performance by criteria of safety, comfort and energy

The project leading to this application has received funding from the European Community Horizon 2020 Framework Programme under grant agreement No. 824333.

efficiency [3]. The ICC tuning in this regard is compound and can be achieved either by configuring the system on the vehicle that is difficult or by using the real systems installed on a test bench. For tuning the integrated systems on the XIL, it is necessary in addition to operate test setups for all controlled actuators simultaneously. A variant of such a complex testing environment and its performance is discussed in [16], [17] and [18].

Hence, to accelerate and expand the area of application of integrated systems in vehicle motion control, it is necessary to introduce methodologies that allow testing of such controllers. As stated before, this might be problematic, especially since controllers involve several sub-components, and sometimes it is not possible or very expensive to place them all in one testing location. This has led to the proposal of a study focusing on a geographically distributed validation system for the integrated control of several active chassis systems, as will be introduced in subsequent sections.

II. Controller design

The structure of the integrated chassis controller is shown in Figure 1. The controller has a multi-level architecture in accordance with the classification from [19], [20]. The proposed controller has five controlled reference states and coordinates the operation of three EV subsystems such as the electric motors, the electro-hydraulic brake system, and the active suspension.

In Figure 1, the abbreviations refer to the following. The reference generator defines a set of reference states for the vehicle body motion: (v, v') the longitudinal velocity and acceleration; (Ψ', Ψ'') the yaw rate and yaw acceleration; (z_b, z_b', z_b'') the vertical displacement, the vertical rate, and the vertical acceleration; $(\Theta, \Theta', \Theta'')$ the pitch angle, the pitch rate, and the pitch acceleration; (Φ, Φ', Φ'') the roll angle, the roll rate, and the roll acceleration. For the ride control targets (e.g. driving comfort, road holding, handling), either the full set of parameters or only several selected parameters are used as the control reference. This means that controller architecture can be adjusted for the desired use case or maneuver. As for the reference state, the vehicle model with reduced body motion has been used.

To detect the maneuver conditions, the reference generator uses the accelerator pedal displacement s_a, the brake pedal displacement s_b, and the steering wheel angle δ. The difference between the measured vehicle states and the values generated by the reference generator after the high-level controller has the dimension and physical meaning of the vertical force, the pitch and roll moment and the yaw moment, which must be generated by the actuators to correct the control error.

The control allocation generates three control vectors to the low-level controllers u_i. The low-level controllers then translate signals for the actuator commands: p_i the brake system pressure; I_i the IWM current and the active suspension valves current. The control allocation is performed taking into account actuator limits $U_{lim}^{low}, U_{lim}^{up}$.

The vehicle model receives torques from the brake system T_b and the IWMs T_m as well as additional vertical forces from the active suspension F_z.

The tasks within the controller layers are divided as follows:

- The reference generator provides a basis for calculating deviations between the vehicle's states and the desired ones. In the developed controller, these errors are $[v_x, \Delta\Psi, \Delta\dot{z}, \Delta\Theta, \Delta\Phi]$, where v_x is the longitudinal velocity error, $\Delta\Psi$ is the yaw error, $\Delta\dot{z}$ is the vertical velocity of the vehicle body and $\Delta\Theta, \Delta\Phi$ are the pitch and roll displacement errors respectively.
- In the high-level controller, five separate PID controllers are used to generate the control demands. Alternatively, another controller architecture can be considered for more precise operation [21] and for reducing the computational requirements to the system in on-board applications [22]. These options can be considered in further studies for corresponding benchmarking.
- In the control allocation part, the demands from the high-level controller are distributed to the actuators using an optimization function. This block generates demanded values, numerically equal to the requests to the low-level controllers.

This configuration has a great potential not only for the current ICC but also can be extended to the architectures with more actuators or sub-systems. In this regard, the control loop can be extended to realize new features for vehicle motion control systems, automated driving capabilities as well as fail-safe and redundancy functionality. On other hand, the proposed controller is very complex for tuning, validation and testing, especially under consideration that all the chassis actuators can be activated at the same time and require a synchronized operation. In this case, traditional hardware-in-the-loop test methods can have insufficient accuracy. In particular, only one sub-system can be tested on a specific HIL platform, and the parameters of other systems could be not fully taken into account in real-time. The solution can be in the replacement of missing hardware components as high-fidelity models and subsequent use of X-in-the-loop technology to involve all acting subsystems in one real-time validation environment.

III. Structure of the testing environment

A. Motivation for the XIL simulation environment

A geographically distributed network of test benches was built to test the developed controller, Figure 2. Each of the systems involved in the integrated chassis controller was represented by a real component. The common component of all involved test setups is the real-time vehicle model operated on the driving simulator. This network configuration allows a very detailed and full real-time testing of the developed ICC strategy.

A test setup with an electric motor serves as the propulsion system in the vehicle model. This makes it possible to evaluate

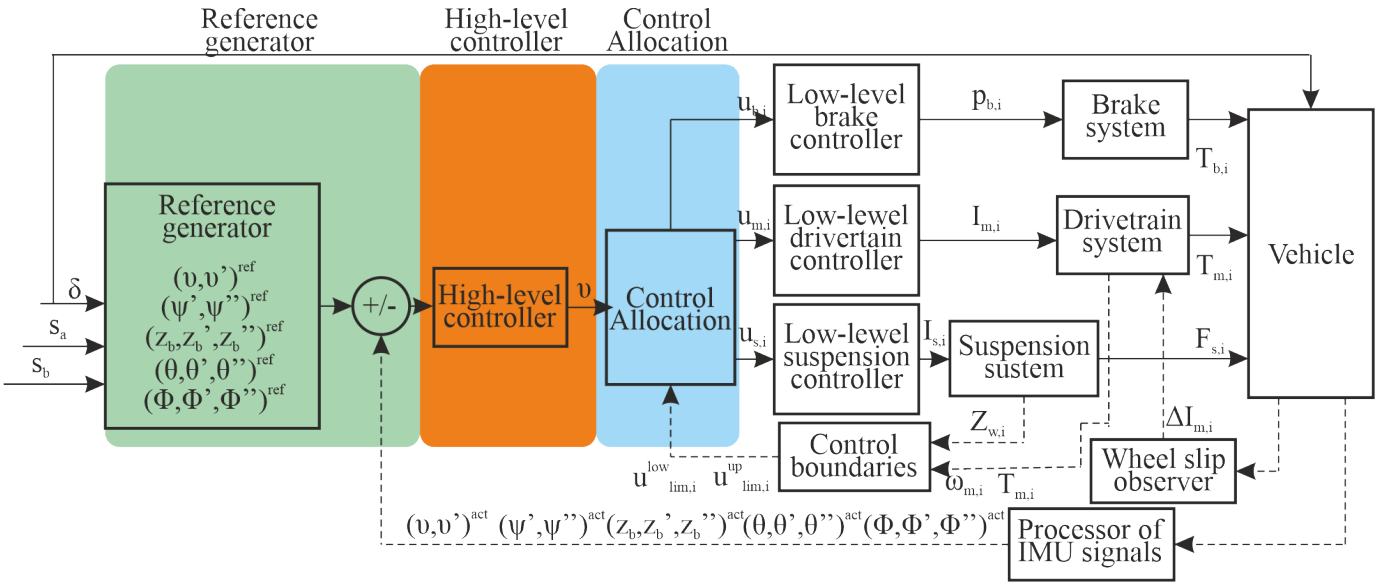

Fig. 1. Developed integrated chassis controller layout.

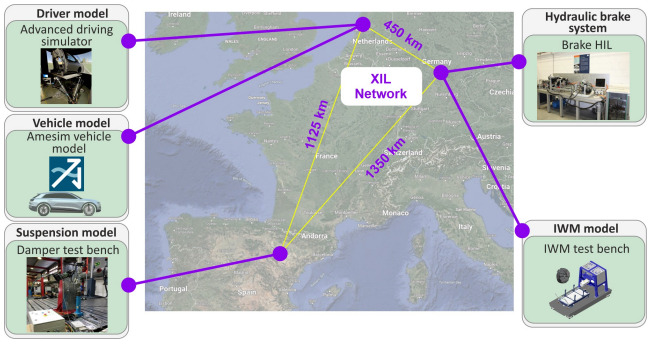

Fig. 2. Proposed testing environment architecture.

the motor's ability to execute the requested commands and validate the control accuracy as well as energy efficiency.

The suspension test bench reproduces a suspension stress simulation scenario and supplements the vehicle model with measured forces during the experiment. This allows the model to accurately reproduce the vertical dynamics of vehicle motion.

The electro-hydraulic brake system test bench allows the consideration of realistic brake pressure. This is required for testing complex manoeuvres involving braking components.

The driving simulator is a key XIL element because it runs a vehicle model. The presence of a moving platform and a driver in the test scenarios make it possible not only to assess the numerical indicators of the vehicle dynamics and control but also to allow the driver to perceive the controller's benefits.

B. Model and environment architecture

It should be ensured that the developed validation environment can precisely reproduce the vehicle dynamics to study various maneuvers and complex controllers. As for the discussed ICC configuration, the architecture can be represented as shown in the diagram in Figure 3. The idea of the controller is to involve the actuators together, so the architecture of the model is designed in parallel sub-models that can be replaced by test benches. Four main components can be highlighted in the environment: (i) Driving simulator and vehicle model, (ii) Brake system test bench, (iii) IWM test bench for powertrain system, (iv) Suspension (damper) test bench.

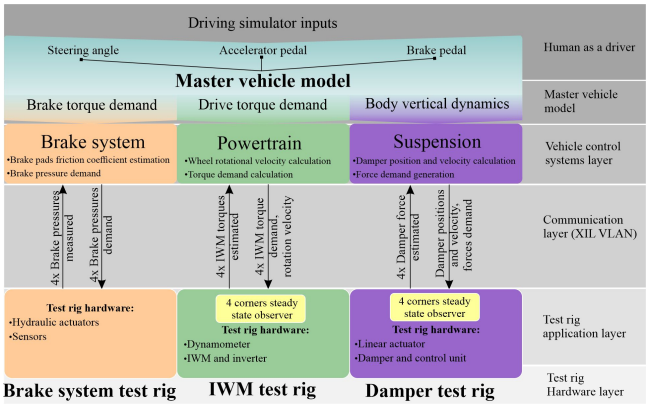

Fig. 3. Model architecture.

The diagram (Figure 3) shows the realized architecture. On the main vehicle model side is the driving simulator, which reproduces the vehicle dynamics for the driver's perception and receives control actions from the operator. The vehicle subsystem control unit converts the driver inputs into signals that can be interpreted by the actuators. This diagram also shows that part of the switching and communication structuring with the test bench is performed by the main application in the vehicle model.

For communication with the brake test bench, the vehicle model requests four pressure signals in the braking system.

The corresponding test bench reproduces the brake pressure signals requested by the vehicle controller and reproduced by the actuators. The sensors on the brake calipers measure the actual brake pressure. The measured values are then transferred to the vehicle model. The hardware test bench measures whether the actuator is able to reproduce the demand generated by the controller. This test method allows consideration of all the physical processes in the system to maximum of accuracy and brings the real-time simulation as close as possible to the dynamics of a real vehicle.

In order to simulate the vehicle powertrain, the dynamometer with the inverter and the IWM is used. The target vehicle model is all-wheel drive, so the sub-system must represent four electric motors. In order to provide four motors in the model with measured values from a single dynamometer and IWM, the application runs a stationary observer on the side of the test bench. The real motor runs an average scenario for testing all IWMs. In this way, the test bench simultaneously and precisely emulates the dynamics of all in-wheel motors of the vehicle.

The suspension test bench provides the replacement of the damper model in the vehicle suspension system with an active suspension actuator. This enables accurate simulation of the vehicle suspension dynamics and measurement of its parameters.

C. Test benches

The conducted experiments were performed on the described network of test benches. Each test bench was connected to the network in real-time. In the designed network, each unit or test bench is included in the architecture shown in Figure 4. The description of the test benches used for this study is briefly described next.

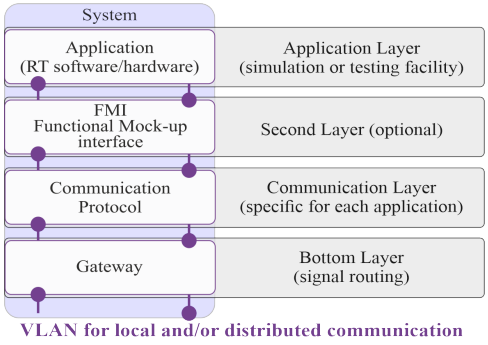

Fig. 4. Model architecture.

1) IWM test bench: The test bench includes installed IWM and inverter (Figure 5) and is connected to the XIL network environment using an additional real-time controller. This controller is responsible for the generation and estimation of wheel torques and is based on the stationary observer. The test bench is running in speed/torque control mode. The torque request is generated by the master simulation of the vehicle model. The torque demand for the test bench motor is defined as the mean value of four torque demands. The velocity of the test bench is controlled by the master simulation and depends on the vehicle velocity.

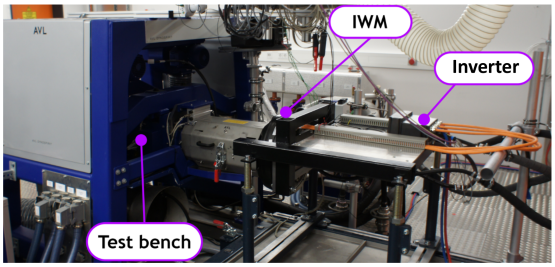

Fig. 5. IWM test bench.

2) Brake system test bench: The test setup of a decoupled electro-hydraulic brake system is used as a hardware subsystem for the master vehicle model. This rig completely replaces a friction brake system from the vehicle model. The test rig consists of four brake mechanisms, hydraulic lines with vehicle-equivalent length, and electro-hydraulic actuators responsible for reproducing the operation of the decoupled brake system, Figure 6.

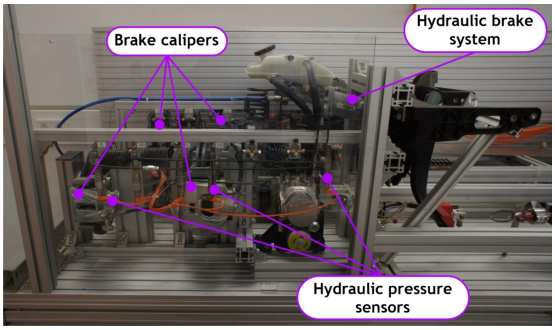

Fig. 6. Electro-hydraulic brake system test bench.

3) Suspension test bench: The suspension test bench node, Figure 7, is composed of the hardware-in-the-loop test setup (shaker) and the real-time computer. To replace the ECU of the active suspension, Rapid Control Prototyping (RCP) hardware is used.

The shaker actuator is running in speed/position control mode. The speed and position are controlled by the linear motor of the test bench and the command is calculated from the real-time vehicle model simulation. The voltage to the valves of the suspension actuator and the pump speed is calculated from the force demand by the master vehicle model.

IV. Results

For the implementation and validation of the proposed controller, an electric sport utility vehicle model, equipped with four independent IWMs, active suspension and an electro-hydraulic decoupled brake system, has been used. Basic vehicle parameters are given in Table I. The reference vehicle is a model which technically corresponds exactly to the model

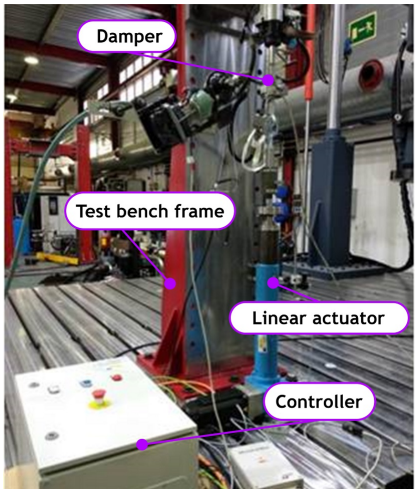

Fig. 7. Suspension test bench.

with an integrated chassis controller, but each subsystem is controlled according to the embedded algorithms.

TABLE I
TEST VEHICLE SPECIFICATION

	Value	Units
Type of powertrain	4 wheel drive IWMs	
Vehicle mass	2578	$[kg]$
Wheel base	1.935	$[m]$
COG to front axle distance	1.494	$[m]$
COG to rear axle distance	1.432	$[m]$
COG height	0.487	$[m]$
Tires	255/55 R19	
Battery voltage	400	$[V]$
Battery capacity	95	$[kWh]$
IWM maximum torque	1500	$[Nm]$
Max speed	181	$[km/h]$

Figure 8 demonstrates the vehicle behavior during the service braking. This maneuver has been performed in the following order. The vehicle accelerates up to velocity $100\ km/h$, keeps this velocity up to steady-state behavior and starts to brake with constant brake pedal actuation corresponding to the 20% of the brake pedal travel. It can be observed that after actuating the brake pedal at the first second of the maneuver the vehicle drives with the almost constant deceleration of $-1\ m/s^2$. At the beginning of the braking, the vehicle body gets some vertical oscillations as well as pitch movement. Figure 8 presents the simulation results for the "baseline" vehicle and vehicle with the ICC described in Section II. It can be seen that the ICC can noticeably decrease the vertical oscillations, the pitch rate of the vehicle, and can reduce an overshoot in the deceleration at the beginning and decrease the longitudinal jerk on the vehicle body. To demonstrate how the controller jointly coordinates the suspension and the IWMs, Figure 9 shows the IWM states. Damper measurements are presented in Figure 10. It can be seen that the controller periodically increases and decreases torque to dump the vertical oscillations and the pitch rate. According to this test, it can be concluded that the developed integrated chassis controller brings a positive effect in terms of driving comfort and safety for the braking maneuver.

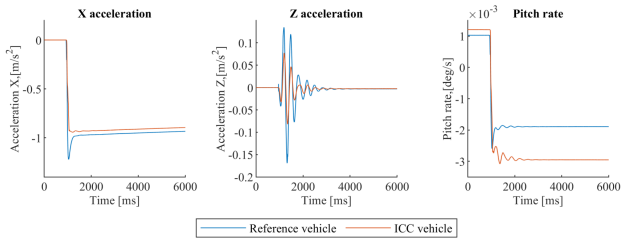

Fig. 8. Results of the simulation of reference vehicle and vehicle with integrated chassis controller for straight-line braking maneuver.

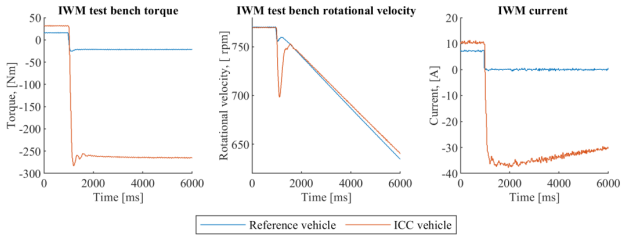

Fig. 9. Powertrain test bench measured parameters during straight-line braking maneuver. Reference vehicle and vehicle with integrated chassis controller are compared.

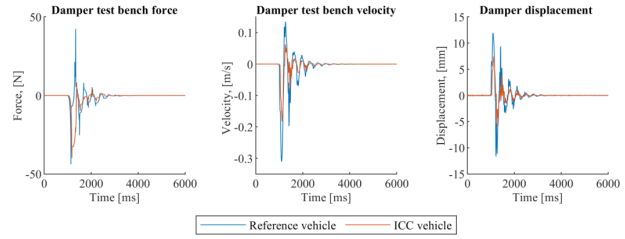

Fig. 10. Damper test bench measured parameters during straight-line braking maneuver. Reference vehicle and vehicle with integrated chassis controller are compared

To study the lateral dynamics under the operation of the integrated chassis controller, a double lane change maneuver according to ISO 3888 has been selected, Figure 11. During the double lane change manoeuvre the vehicle is rapidly shifting to a neighbouring lane and returning straight back. This can simulate a collision avoidance situation and allows the evaluation of vehicle dynamics in a critical driving case. The maneuver is performed at the velocity of $65\ km/h$. The maneuver ends when the vehicle has returned to its lane. It is noticeable that the controller allows keeping slightly higher longitudinal acceleration of the vehicle and reduces oscillations that positively affect both the tire-road holding and the perception of the driver. Also, improvements can be noticed in the roll and pitch dynamics.

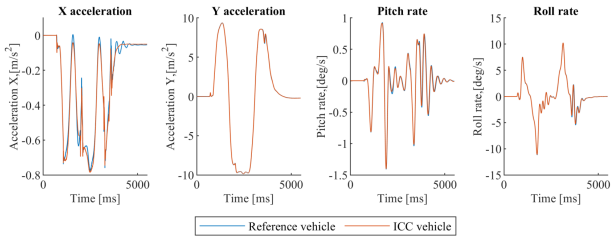

Fig. 11. Results of the simulation of reference vehicle and vehicle with integrated chassis controller for double lane change maneuver 65 km/h

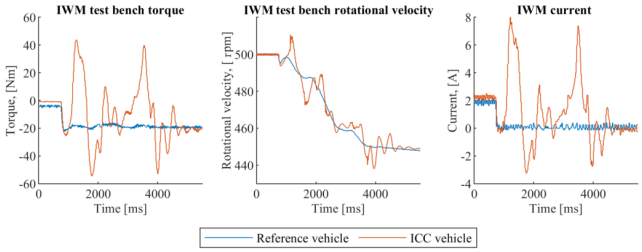

Fig. 12. Powertrain test bench: measured parameters during double lane change maneuver on 65 km/h. Reference vehicle and vehicle with integrated chassis controller are compared

The controller operation is also illustrated with the results from the IWM test bench, Figure 12. The IWMs operation slightly changes and reduces the force and the displacement of the damper on the suspension test bench. This is illustrated with the measurements shown in Figure 13.

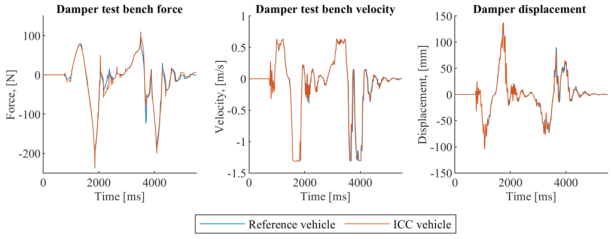

Fig. 13. Suspension test bench: measured parameters during double lane change maneuver on 65 km/h. Reference vehicle and vehicle with integrated chassis controller are compared

To demonstrate ICC effect for a more critical situation, the double lane change maneuver has been repeated for 85 km/h. A lower speed maneuver does not allow the vehicle to reach its performance limits, and the controller's ability to fully control the vehicle may seem insignificant. By higher velocities, in the contrast, the reference vehicle does not pass the maneuver. The ICC operation, which takes into account the vehicle's operating limits, desired yaw rate and actuator constraints, allows the vehicle to remain steerable. The vehicle dynamics for such a maneuver are shown in Figure 14. The greater deceleration of the vehicle during the first lane change is caused by the vehicle driving harder than the reduced degrees of freedom model allows, for this reason, the controlling allocation reduces the velocity taking into consideration the limits. In the meantime, the vehicle achieves the same lateral acceleration and yaw rate. Therefore, the vehicle passes this maneuver successfully.

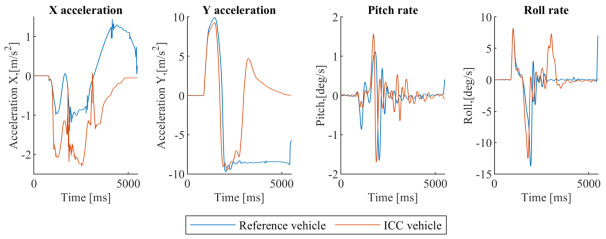

Fig. 14. Results of the simulation of reference vehicle and vehicle with integrated chassis controller for double lane change maneuver 85 km/h

To evaluate the effect from the controller, Table II shows the key performance indicators (KPI) calculated for investigated maneuvers. The KPI for Comfort is based on ISO 2631 and the KPI for Safety corresponds to the RMSE value of the wheel load variations. The safety criterion is evaluated according to the following equation:

$$RMSE = \frac{1}{4}\sum_{r=1}^{m,j}\sqrt{\frac{1}{n}\sum_{k=1}^{n}(F_{wheeli} - F_{wheelstandi})^2} \quad (1)$$

where $F_(wheeli)$ is the vertical load on a tyre; $F_{wheelstandi}$ is the vertical load on that tyre in static conditions; the indices "m,j" are for the front and rear wheels respectively.

The following criteria for comfort evaluation are suggested by ISO 2631:

- W_k - weighted RMS value of vertical acceleration $(k = 1)$.
- W_e - weighted RMS value of pitch acceleration $(k = 0.4)$.
- W_d - weighted RMS value of roll acceleration $(k = 0.63)$.

All the maneuver were conducted five times to avoid inaccuracies, and average values are summarized in Table II. A decrease in the numerical values in Table 2 indicates that KPIs for ICC evaluation would correspond to an improvement in the quality/performance of the manoeuvre in relation to the specific vehicle feature (comfort or safety).

TABLE II
KEY PERFORMANCE INDICATORS FOR SAFETY AND COMFORT

Manoeuvre	Setup	KPI Comfort	KPI safety
Straight Line Braking	Reference	1.296	1.043
	ICC	0.949	0.967
Double Lane Change at 65 km/h	Reference	19.035	0.989
	ICC	20.099	0.997
Double Lane Change at 85 km/h	Reference	64.724	0.983
	ICC	17.872	0.995

V. Conclusion

This paper proposes a method to validate controller performance using a geographically distributed network of X-in-the-loop test benches. The method is demonstrated based on an integrated chassis controller for a four-wheel drive EV with active suspension and an electro-hydraulic braking system. The practical importance lies in the demonstrated ability of such test environment architecture to reproduce a vehicle model, engage multiple test benches and simulate controllers of complex architecture. Practical validation of the controller proves the ability to increase driving comfort and increase the key performance indicators reflecting the driving safety across various test scenarios related to the longitudinal and lateral dynamics.

References

[1] E. Katsuyama, "Decoupled 3d moment control using in-wheel motors," *Vehicle System Dynamics - VEH SYST DYN*, vol. 51, pp. 1–14, 01 2012.

[2] B. Shyrokau and D. Wang, "Control allocation with dynamic weight scheduling for two-task integrated vehicle control," in *Proc. 11th Int. Symp. Adv. Vehicle Control*, 2012, pp. 1–6.

[3] B. Shyrokau, D. Wang, D. Savitski, K. Hoepping, and V. Ivanov, "Vehicle motion control with subsystem prioritization," *Mechatronics*, vol. 30, pp. 297–315, 2015. [Online]. Available: https://www.sciencedirect.com/science/article/pii/S0957415814001792

[4] L. Hott, V. Ivanov, K. Augsburg, V. Ricciardi, M. Dhaens, M. A. Sakka, K. Praet, and J. V. Molina, "Ride blending control for awd electric vehicle with in-wheel motors and electromagnetic suspension," in *2020 IEEE Vehicle Power and Propulsion Conference (VPPC)*, 2020, pp. 1–5.

[5] D. Savitski, V. Ivanov, B. Shyrokau, J. De Smet, and J. Theunissen, "Experimental study on continuous abs operation in pure regenerative mode for full electric vehicle," *SAE Int. J. Passeng. Cars-Mech. Syst*, vol. 8, no. 1, pp. 364–369, 2015.

[6] F. Pretagostini, L. Ferranti, G. Berardo, V. Ivanov, and B. Shyrokau, "Survey on wheel slip control design strategies, evaluation and application to antilock braking systems," *IEEE Access*, vol. 8, pp. 10 951–10 970, 2020.

[7] C. Lin, X. Guo, and X. Pei, "A novel coordinated algorithm for vehicle stability based on optimal guaranteed cost control theory," *SAE International Journal of Vehicle Dynamics, Stability, and NVH*, vol. 4, no. 10-04-03-0022, pp. 327–339, 2020.

[8] N. Aouadj, K. Hartani, and M. Fatiha, "New integrated vehicle dynamics control system based on the coordination of active front steering, direct yaw control, and electric differential for improvements in vehicle handling and stability," *SAE International Journal of Vehicle Dynamics, Stability, and NVH*, vol. 4, no. 10-04-02-0009, pp. 119–133, 2020.

[9] S. Kolte, A. K. Srinivasan, and A. Srikrishna, "Development of decentralized integrated chassis control for vehicle stability in limit handling," *SAE International Journal of Vehicle Dynamics, Stability, and NVH*, vol. 1, no. 2016-01-8106, pp. 1–10, 2016.

[10] V. Mazzilli, S. De Pinto, L. Pascali, M. Contrino, F. Bottiglione, G. Mantriota, P. Gruber, and A. Sorniotti, "Integrated chassis control: Classification, analysis and future trends," *Annual Reviews in Control*, vol. 51, pp. 172–205, 2021. [Online]. Available: https://www.sciencedirect.com/science/article/pii/S1367578821000055

[11] K. Augsburg, S. Gramstat, R. Horn, V. Ivanov, H. Sachse, and B. Shyrokau, "Investigation of brake control using test rig-in-the-loop technique," in *SAE 2011 Annual Brake Colloquium*, no. 2011-01-2372, 2011.

[12] L. Heidrich, B. N. Shyrokau, D. Savitski, V. G. Ivanov, K. Augsburg, and D. W. Wang, "Hardware-in-the-loop test rig for integrated vehicle control systems," *IFAC Proceedings Volumes*, vol. 46, pp. 683–688, 2013.

[13] V. Ivanov, K. Augsburg, C. Bernad, M. Dhaens, M. Dutré, S. Gramstat, P. Magnin, V. Schreiber, U. Skrt, and N. Van Kelecom, "Connected and shared x-in-the-loop technologies for electric vehicle design," *World Electric Vehicle Journal*, vol. 10, no. 4, 2019. [Online]. Available: https://www.mdpi.com/2032-6653/10/4/83

[14] V. Schreiber, V. Ivanov, K. Augsburg, M. Noack, B. Shyrokau, C. Sandu, and P. S. Els, "Shared and distributed x-in-the-loop tests for automotive systems: Feasibility study," *IEEE Access*, vol. 6, pp. 4017–4026, 2018.

[15] J. Zhao, P.-K. Wong, X. Ma, and Z. Xie, "Chassis integrated control for active suspension, active front steering and direct yaw moment systems using hierarchical strategy," *Vehicle System Dynamics*, vol. 55, pp. 1–32, 10 2016.

[16] S. Moten, F. Celiberti, M. Grottoli, A. van der Heide, and Y. Lemmens, "X-in-the-loop advanced driving simulation platform for the design,development, testing and validation of adas," in *2018 IEEE Intelligent Vehicles Symposium (IV)*, 2018, pp. 1–6.

[17] S. Riedmaier, J. Nesensohn, C. Gutenkunst, T. Düser, B. Schick, and H. Abdellatif, "Validation of x-in-the-loop approaches for virtual homologation of automated driving functions," 05 2018.

[18] G. Tibba, C. Malz, C. Stoermer, N. Nagarajan, L. Zhang, and S. Chakraborty, "Testing automotive embedded systems under x-in-the-loop setups," in *2016 IEEE/ACM International Conference on Computer-Aided Design (ICCAD)*, 2016, pp. 1–8.

[19] J. Zhao, P. K. Wong, X. Ma, and Z. Xie, "Chassis integrated control for active suspension, active front steering and direct yaw moment systems using hierarchical strategy," *Vehicle System Dynamics*, vol. 55, pp. 103 – 72, 2017.

[20] G. Chen and D. Zhang, "Research on integrated chassis control strategy for four-wheel independent control electric vehicle," *SAE Technical Papers*, 09 2014.

[21] K. Miyahara, H. Fujimoto, Y. Hori, and V. Ivanov, "Performance benchmark of yaw rate controllers by active front steering: Comparative analysis of model predictive control, linear quadratic integral control and yaw moment observer," in *IECON 2019 - 45th Annual Conference of the IEEE Industrial Electronics Society*, vol. 1, 2019, pp. 473–478.

[22] C. Fu, R. Hoseinnezhad, K. Li, M. Hu, F. Huang, and F. Li, "Vehicle integrated chassis control via multi-input multi-output sliding mode control," in *2018 International Conference on Control, Automation and Information Sciences (ICCAIS)*, 2018, pp. 355–360.